



Forming oriented organic crystals from amorphous thin films on patterned substrates via solvent-vapor annealing

Debra J. Mascaro ^{a,1}, Mark E. Thompson ^b,
Henry I. Smith ^c, Vladimir Bulović ^{c,*}

^a Department of Materials Science and Engineering, Massachusetts Institute of Technology, Cambridge, MA 02139, USA

^b Department of Chemistry, University of Southern California, Los Angeles, CA 90089, USA

^c Department of Electrical Engineering and Computer Science, Massachusetts Institute of Technology, Cambridge, MA 02139, USA

Received 21 March 2005; received in revised form 20 July 2005; accepted 25 July 2005

Available online 26 August 2005

Abstract

The challenge of generating crystals of organic materials has been pursued by many research groups who aim to develop materials sets for active electronic and optoelectronic devices, including field-effect transistors [C.D. Dimitrakopoulos, P.R.L. Malenfant, *Adv. Mater.* 14 (2002) 99; H.E. Katz, Z. Bao, *J. Phys. Chem. B* 104 (2000) 671; Y.Y. Lin, D.J. Gundlach, S.F. Nelson, T.N. Jackson, *IEEE Trans. Electron Dev.* 44 (1997) 1325], photodetectors [P. Peumans, V. Bulović, S.R. Forrest, *Appl. Phys. Lett.* 76 (2000) 2650] and optical modulators [S.R. Marder, J.W. Perry, C.P. Yakymyshyn, *Chem. Mater.* 6 (1994) 1137]. Here we describe a method for in-plane growth of millimeter-scale crystalline organic needles from initially amorphous thin films of the molecular organic semiconductor tris(8-hydroxyquinoline)aluminum (Alq₃). The needles form when the vacuum-deposited amorphous films are exposed to chloroform vapor at room temperature and pressure, and can be as large as several microns thick, several microns wide, and one centimeter long (limited in length by the substrate dimensions). As such, the Alq₃ needles are more than 1000 times longer than any previously reported organic crystals formed via a similar solvent-vapor annealing process [F. Iwatsu, T. Kobayashi, N. Uyeda, *J. Phys. Chem.* 84 (1980) 3223; F. Iwatsu, *J. Cryst. Growth* 71 (1985) 629; A.M. Hor, R.O. Loutfy, *Thin Solid Films* 106 (1983) 291; B.A. Gregg, *J. Phys. Chem.* 100 (1996) 852; J.C. Conboy, E.J.C. Olson, D.M. Adams, J. Kerimo, A. Zaban, B.A. Gregg, P.F. Barbara, *J. Phys. Chem. B* 102 (1998) 4516; M. Brinkmann, J.C. Wittmann, C. Chaumont, J.J. Andre, *Thin Solid Films* 292 (1997) 192; F. Toffolo, M. Brinkmann, O. Greco, F. Biscarini, C. Taliani, H.L. Gomes, I. Aiello, M. Ghedini, *Synth. Met.* 101 (1999) 140]. Moreover, the Alq₃ needles are spatially separated from one another and oriented with their long axes parallel to lithographically pre-defined periodic submicron grooves in the substrate surface.

© 2005 Published by Elsevier B.V.

* Corresponding author. Tel.: +1 617 253 7012; fax: +1 617 452 5110.

E-mail address: bulovic@mit.edu (V. Bulović).

¹ Present address: Department of Mechanical Engineering, University of Utah, Salt Lake City, UT 84112, USA.

PACS: 81.10.-h; 78.66.Qn

Keywords: Organic single crystal; Crystal growth; Solvent-vapor annealing; Organic thin film morphology; Tris(8-hydroxyquinoline)aluminum (Alq_3)

1. Introduction

The growth of free-standing organic crystals millimeters in size has been previously demonstrated by resublimation [13–18] and solvent recrystallization [5,13,14], and in a few studies discrete active devices have been fabricated using such crystals [19–22]. However, in order to enable monolithic integration of active organic components [1–5] into all-organic or hybrid integrated systems, it is necessary to form organic crystals in the plane of a large area (cm^2) substrate. The deposition of high purity molecular organic materials onto planar substrates is most often accomplished by vacuum sublimation, but the deposited thin films are typically amorphous or at best polycrystalline with grain sizes on the scale of microns [23–26]. Substrate temperatures are often elevated during deposition in order to improve crystallinity or select a particular crystalline phase [3,11,23–28]. In addition, post-deposition thermal treatment, solvent exposure, and solvent-vapor exposure have been shown to induce grain growth as well as amorphous-to-crystalline or polymorphic transformations in molecular organic thin films [6–12,29,30]. In the case of solvent-vapor annealing, a solvent in which the thin film material has only slight solubility is typically used. The results reported here differ in that Alq_3 is readily soluble in common organic solvents including chloroform.

We demonstrate the crystal formation method using Alq_3 since it is among the most extensively studied molecular organic semiconductors. Vacuum-sublimed thin films of Alq_3 are typically amorphous and have been shown to be morphologically stable under inert atmosphere and room temperature conditions [31]. It has been observed, however, that micron-scale disk-like clusters of crystals form [32] when amorphous thin films of Alq_3 are thermally annealed above the Alq_3 glass transition temperature ($T_g = 175^\circ\text{C}$) [33]. More-

over, vacuum evaporation of Alq_3 onto heated glass substrates pre-rubbed with polytetrafluoroethylene (PTFE) was shown to yield polycrystalline Alq_3 films of planar $\sim 1\text{--}2\ \mu\text{m}$ crystallites [23]. In the PTFE study, the Alq_3 crystallites were also oriented relative to the PTFE sliding direction, with the orientation primarily attributed to the van der Waals interaction of Alq_3 molecules with the aligned PTFE chains. Such ordering is driven by the minimization of interfacial tension between the crystal and the substrate, and has been demonstrated in other studies that used lithographically-defined periodic surface relief to influence the growth and orientation of inorganic crystalline overlayers [34,35], to uniaxially orient liquid crystalline molecules over large areas [36], and to generate long-range order in self-assembling block copolymer thin films [37].

Similar to thermally-assisted Alq_3 crystal formation [23,32], exposure of Alq_3 films to acetone vapor was previously reported to yield micron-scale crystallized regions [12]. In this study we demonstrate that much larger (millimeter-scale) Alq_3 crystalline needles can be formed by solvent-vapor annealing amorphous Alq_3 films on submicron surface-relief gratings.

2. Experimental

Interference lithography was used to fabricate grating lines in Si or SiO_2 with periods ranging from 180 nm to 300 nm and etch depths from 30 nm to 70 nm. The trilayer resist stack consisted of an anti-reflection coating (ARC) layer, an evaporated silica interlayer, and a photoresist layer, with the layers deposited sequentially onto silicon or thermally oxidized silicon wafers. A 325 nm wavelength HeCd laser was used to expose grating lines in the resist. After exposure and development of the resist, the pattern was transferred through

the silica interlayer and ARC layer and into the Si or SiO₂ via reactive ion etching. After removal of the residual resist stack by cleaning in 5:1:1 H₂O:H₂O₂:NH₄OH at 80 °C for ~10 min, a square-wave grating topography remained in the Si or SiO₂.

After the patterned wafers were diced into ~cm² pieces, the substrates were cleaned via the following steps: ultrasonication in dilute detergent, ultrasonication in deionized water, ultrasonication in acetone, immersion in boiling 1,1,1-trichloroethane, ultrasonication in acetone, and immersion in boiling 2-propanol. The substrates were then dried in a stream of nitrogen and further cleaned by UV-ozone treatment for 30 min. The substrates were subsequently treated with octadecyltrichlorosilane (OTS). The vapor phase OTS treatment was accomplished by placing the substrates in a vessel together with a crucible containing ~0.03 ml of OTS. The vessel was evacuated to a pressure of <1 Torr and heated to 120 °C in an oil bath for ~2 h. The OTS-treated substrates were hydrophobic, with contact angles (measured on unpatterned substrates) of ~87°.

Alq₃ films of 10–20 nm thickness were deposited by thermal evaporation in vacuum (<10⁻⁶ Torr) onto room temperature substrates at rates of 0.1–0.3 nm/s as measured by a quartz crystal thickness monitor. Following the evaporation of Alq₃, the substrates were placed in a glass jar together with a beaker of chloroform, and the jar was sealed with a Teflon-lined cap. Exposure times ranged from several hours to two days. The dimensions of the Alq₃ needles formed via chloroform-vapor annealing were characterized by optical microscopy (needle length), and scanning electron microscopy (SEM) and atomic force microscopy (AFM) (needle width, thickness). Optical properties of the needles were investigated via fluorescence microscopy and confocal microscopy (365 nm excitation wavelength).

In order to monitor the growth of Alq₃ crystals during chloroform-vapor exposure, an alternate annealing chamber was constructed from stainless steel and quartz vacuum components. A stereomicroscope was used to view a substrate mounted beneath a quartz view port, and video was captured via an attached CCD camera.

3. Experimental results

Exposure of the Alq₃ thin films to chloroform vapor for times ranging from several hours to two days results in the formation of elongated and oriented Alq₃ needles such as those shown in the optical and SEM micrographs of Fig. 1. The narrowest needles are two to three hundred nanometers wide, spanning a single grating groove (Fig. 3(c)), while the widest are several microns wide and span tens of grooves (Fig. 1(d)). Needle thicknesses range from one hundred nanometers to several microns, exceeding the depth of the grating grooves by as much as a factor of 50, and the thickness of the initial amorphous Alq₃ film by as much as a factor of 200. The needles are often 1000 times longer than they are wide or thick, ranging in length from hundreds of microns to one centimeter (the size of the substrate). In some cases the needles extend several microns beyond the substrate edge, retaining their elongated geometry, consistent with the growth of a crystal (Fig. 1(c)).

The distinct facets (Fig. 1(d)) and diamond-shaped cross sections (Fig. 1(e)) of the Alq₃ needles are also indicative of crystallinity. The optical smoothness of the needle facets is evidenced in fluorescence micrographs that show waveguiding of the Alq₃ fluorescence with outcoupling occurring at the needle edges and defects (Fig. 1(c)). Polarized fluorescence measurements show a change in luminescence intensity with polarization angle, with a maximum at ~15° from the long axis of the needle (Fig. 2(a)). Fluorescence spectra of the crystal needles, obtained via confocal microscopy, peak at $E_{\text{peak}} = 2.36$ eV ($\lambda_{\text{peak}} = 525$ nm) in agreement with the previously reported spectrum of polycrystalline α -Alq₃ (Fig. 2(b)) [38].

Not all of the Alq₃ is incorporated into the needles during the chloroform-vapor exposure. In fact, two regimes of residual Alq₃ are observed alongside the needles (Fig. 3). In the first regime (“Regime I” in Fig. 3), the Alq₃ is in the form of ~100 nm diameter convex globules and microcrystallites that cluster in the grating grooves to form ~1 μ m long features (Fig. 3(d)). The Regime I residual Alq₃ is visible in the optical micrographs as shade/color variations (darker region on the left in Fig. 1(a), green background in Fig. 1(b)).

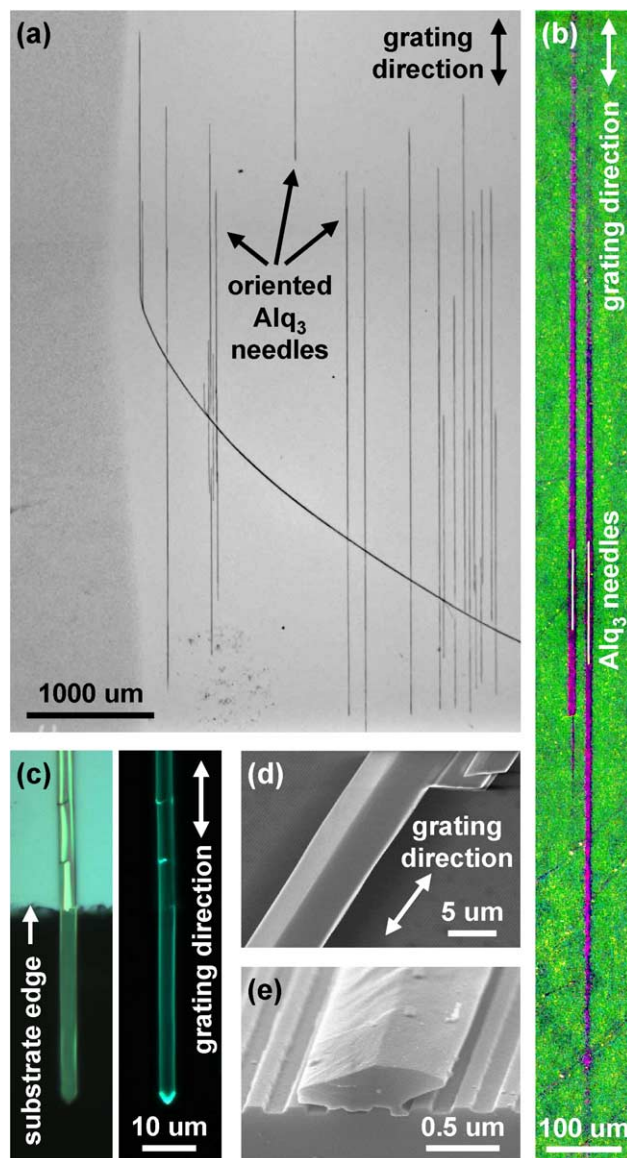


Fig. 1. Alq₃ crystalline needles formed by exposure of amorphous Alq₃ thin films to chloroform vapor at room temperature. (a) Optical micrograph of oriented Alq₃ crystal needles that formed from a 10 nm thick film of amorphous Alq₃. (b) False-color optical micrograph showing Alq₃ needles colored white, regions containing “Regime I” residual Alq₃ colored green, and regions containing “Regime II” residual Alq₃ colored magenta. (c) Optical micrograph (left) and fluorescence micrograph (right, 365 nm excitation wavelength) of an Alq₃ needle that extends ~35 μm beyond the substrate edge. (d) SEM micrograph (top view) showing the distinct facets of an Alq₃ needle. (e) SEM micrograph showing the typical diamond-shaped cross section of an Alq₃ needle.

Although it appears from the optical micrographs that the Alq₃ has been cleared from the substrate in the vicinity of the needles (bulk of the substrate in Fig. 1(a), elongated magenta regions in

Fig. 1(b)), SEM and AFM characterization reveals a second regime of residual Alq₃ (“Regime II” in Fig. 3). In contrast to the non-wetting globules and microcrystallites of Regime I, the residual

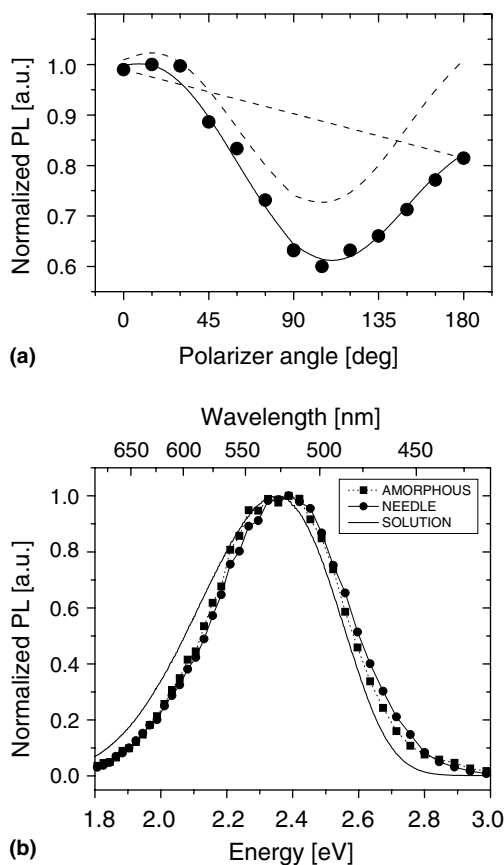


Fig. 2. Fluorescence of Alq₃ needles. (a) Plot of the normalized photoluminescence (PL) intensity (365 nm excitation wavelength) as a function of polarizer angle, where 0° corresponds to the polarizer aligned with the long axis of the needle. The decrease in fluorescence intensity from 0 to 180° is due to gradual photooxidation of the Alq₃ during the measurement as indicated by the straight dashed line. The sinusoidal response of PL with polarizer angle and the composite of the PL response and the gradual oxidation are plotted in dashed and solid lines, respectively. (b) Fluorescence spectra (365 nm excitation wavelength) of an as-deposited Alq₃ thin film and an Alq₃ crystal needle, obtained via confocal microscopy. The solution fluorescence spectrum (408 nm excitation wavelength) of Alq₃ in chloroform is also plotted.

Alq₃ in the grooves adjacent to the needles appears fluid-like and wets the substrate, forming strips that span individual grating grooves, and smaller droplets clinging to the groove sidewalls (Fig. 3(c) and (d)). In general, the area of the Regime II region surrounding a needle increases with increasing needle size (e.g., compare Fig. 1(a) and 1(b)), and

these regions are elongated in the grating direction (Fig. 1(b)).

Time-based experiments provide insight into the relationship between the Regime I and Regime II Alq₃ morphologies. The structural evolution shown in the Fig. 4 AFM images was produced by exposing identical Alq₃ thin film samples to chloroform vapor for different lengths of time. The as-deposited Alq₃ film shown in Fig. 4(a) is continuous, conforming to the underlying grating, but is rough due to the OTS pre-treatment. (Unlike Alq₃ on clean Si or SiO₂, which forms smooth, continuous films even when very thin (~1 nm), Alq₃ on OTS-treated surfaces forms isolated islands during the initial stages of growth due to increased interfacial tension.) Film continuity is lost during the first 5 min of exposure to chloroform vapor (Fig. 4(b)). After exposure for 30 min, the Alq₃ resides primarily in the grating grooves in the form of Regime I globules and microcrystallites (Fig. 4(c)). Increasing the exposure time to 60 min yields aggregation of the globules/microcrystallites to form micron-long clusters (Fig. 4(d), see also Fig. 3(d)). During an additional 30 min of exposure, the aggregated globules/microcrystallites begin to dissolve into Regime II liquescent strips that extend along the grating grooves (Fig. 4(e), see also Fig. 3(d) inset). Chloroform uptake in the Alq₃ film should increase with prolonged vapor exposure, suggesting that the Alq₃ transitions from Regime I to Regime II with increasing chloroform concentration.

Most of our experiments were carried out as described above, with samples characterized after being removed from the annealing chamber. While it is conceivable that the evaporation of chloroform upon removal from the saturated chamber atmosphere may influence or even produce the observed Alq₃ structures, we have disproved the latter by monitoring the growth of Alq₃ needles during chloroform-vapor exposure as described in the Experimental section. The sequence of optical micrographs shown in Fig. 5 corresponds to a 50 nm thick Alq₃ film on a grating pre-treated with phenyltrichlorosilane. In this case, chloroform-vapor exposure produced a tree-like structure of crystalline Alq₃ with branching needles aligned predominantly parallel to the grating direction.

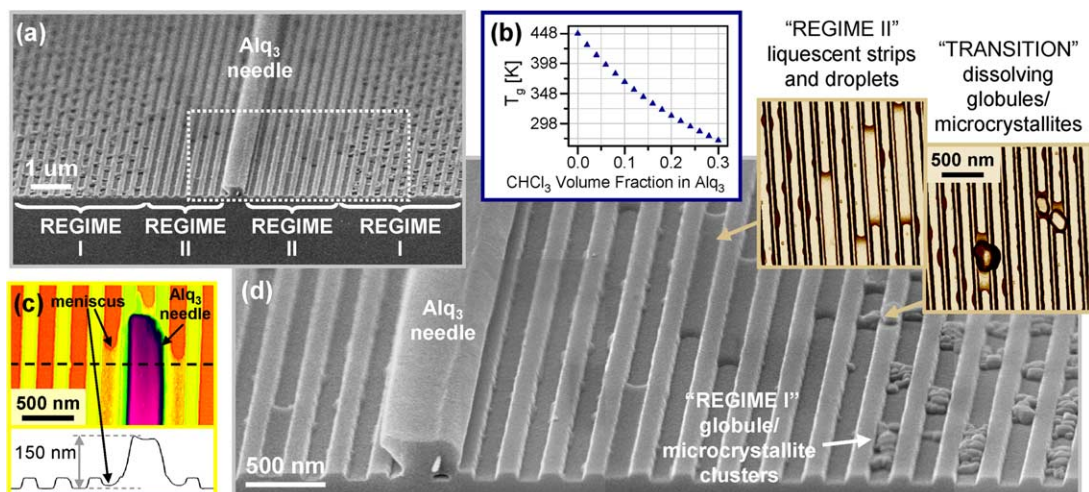


Fig. 3. Residual Alq₃ structural regimes. (a) SEM micrograph of an Alq₃ needle (in cross section) showing the morphological transition of the residual Alq₃ near the needle with Regimes I and II indicated. (b) Plot of the predicted T_g of Alq₃ solvated with chloroform as a function of chloroform volume fraction, calculated from Eq. (1). (c) AFM height image of the tip of an Alq₃ needle showing liquescent Alq₃ in the immediately adjacent grooves. (d) SEM micrograph corresponding to the dashed box in (a), and AFM height image insets (displayed with top illumination to highlight edges and contours).

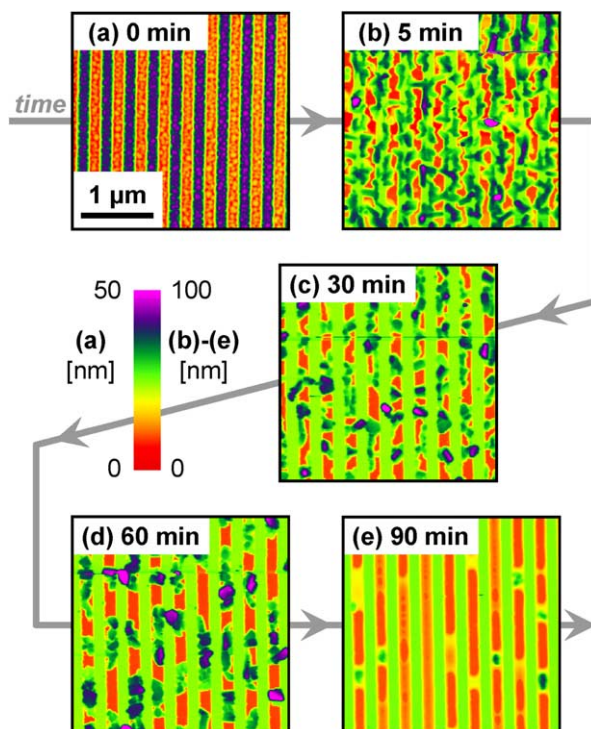


Fig. 4. AFM height images showing the structural evolution of Alq₃ thin films when exposed to chloroform vapor for increasing times. The initial film was 10 nm thick, deposited onto an OTS-treated surface-relief grating.

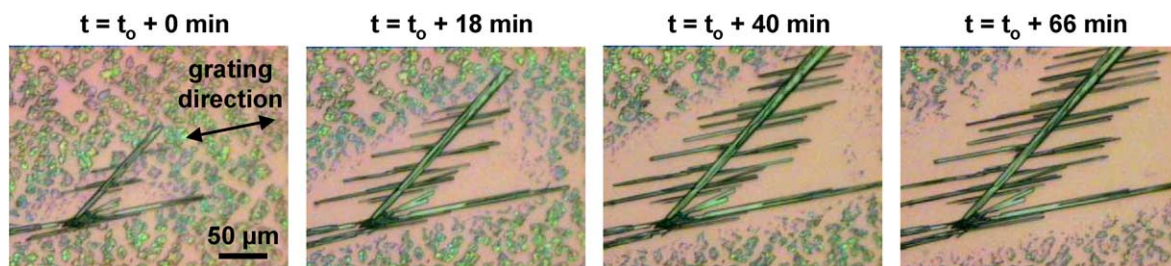


Fig. 5. Time-lapse optical micrographs showing the growth of Alq₃ crystalline needles during chloroform-vapor exposure. The initial film was 50 nm thick, deposited onto a phenyltrichlorosilane-treated surface-relief grating.

During the course of an hour-long exposure to chloroform vapor, new branches formed, the “trunk” and branches grew larger, and the surrounding “cleared” region increased in area.

As evidenced by the Fig. 5 micrographs, the formation of Alq₃ crystals via chloroform-vapor exposure is not limited to OTS-treated substrates. In fact, we have also observed millimeter-scale Alq₃ crystals on untreated Si gratings and on gratings having a thin (<10 nm) coating of copper phthalocyanine (deposited by thermal evaporation immediately prior to deposition of the Alq₃ film), but we have not studied these substrate systems as thoroughly as the OTS-treated system. We have also observed formation of Alq₃ crystalline needles on unpatterned substrates; however, these needles are generally slower to form, fewer in number, shorter, and have random in-plane orientations, highlighting the influence of the grating grooves on both nucleation and mass transport.

The chloroform uptake of Alq₃ thin films was quantified using a quartz crystal thickness monitor. A beaker of chloroform was placed beneath the thickness monitor such that the quartz crystal was ~1 cm above the chloroform level. The beaker and thickness monitor were capped with aluminum foil to simulate the sealed annealing chamber. This experiment was performed first on a blank quartz crystal, and was then repeated for the same crystal after deposition of a 50 nm thick film of Alq₃. The maximum mass increase after exposure to chloroform vapor was 10 times larger for the Alq₃ coated crystal than for the blank quartz crystal, and corresponds to a chloroform mass fraction of 0.21.

4. Discussion

Previous reports of solvent-vapor annealing of amorphous or polycrystalline molecular organic thin films focused on metal phthalocyanines [6–8,11] and perylene derivatives [9,10], where the goal was to improve photoactivity for applications such as xerography or photovoltaic devices. The films tended to have low solubility in the annealing solvents, and adsorption of solvent molecules during solvent-vapor exposure was presumed to result in a saturated solvent solution on the film surface. Two main mechanisms were proposed for the observed crystalline transformations. First, solvent molecules may interact electronically with the thin film molecules to change their π -electron distributions, triggering a change in molecular packing. Alternately, adsorbed solvent molecules may cause a relaxation of a metastable crystal lattice or an increase in molecular motility at the surface of an amorphous thin film, thereby enabling nucleation of a stable crystalline form. The latter mechanism was consistent with observations that (1) transformation rates tend to increase with increasing solubility [6] and (2) similar transformations can be activated via thermal treatment [11]. In cases where an increase in crystal size was observed (rather than a polymorphic transition), the growth was attributed to Ostwald ripening, with the solvent solution serving as a transport medium. The largest reported crystals were a few microns in length.

Although we observe some similarities in the structural changes of vapor-annealed Alq₃ films, the higher solubility of Alq₃ in chloroform

influences the active mechanisms. First, adsorbed chloroform molecules have an increased tendency to diffuse into the amorphous Alq₃ film, enabling “bulk” rather than surface transformations. The imbibed chloroform imparts motility to the Alq₃ molecules via a plasticization effect, whereby the T_g of a glassy material is reduced by the presence of low molecular weight additives (such as solvent molecules). The effect of plasticization on T_g can be estimated from semi-empirical equations based on free-volume considerations [39]:

$$T_g \approx \frac{T_{go}}{1 + \left(\frac{T_{go}}{T_{gs}} - 1\right) \Phi_s} \quad (1)$$

$$T_{gs} \approx \frac{2}{3} T_{ms} \quad (2)$$

where T_{go} and T_{gs} are the glass transition temperatures of the pure glassy material and pure solvent, respectively, and Φ_s is the volume fraction of the solvent. The melting temperature of the solvent T_{ms} is used to estimate T_{gs} using the relationship given in Eq. (2). Using $T_{go} = 448$ K for Alq₃ and $T_{ms} = 210$ K for chloroform, the Alq₃ T_g is calculated to drop below room temperature (298 K) when the film is 23% chloroform by volume (Fig. 3(b)). This value is in good agreement with our quartz crystal measurement of 21% by mass chloroform uptake for a 50 nm thick Alq₃ film. In order to compare mass and volume fractions, we are assuming that the density of the film does not change significantly with chloroform uptake; that is to say, the density of chloroform in Alq₃ is assumed to be closer to the density of neat Alq₃ (1.16 g/cm³ [40]) than to the density of neat chloroform (1.48 g/cm³) due to less dense packing in the solvated structure. The reduction of T_g via chloroform uptake provides the molecular motility necessary for the Alq₃ to minimize interfacial tension by dewetting from the substrate (Fig. 4(b)), and overall free-energy by forming the Regime I globule/microcrystallite clusters (Figs. 3(d), 4(c) and (d)), both at room temperature. Nucleation of the larger crystalline needles also likely results from the reduced Alq₃ T_g , although the seeding process is not yet understood.

Initially the level of chloroform uptake is such that, in effect, chloroform is dissolved in Alq₃

“solvent”. However, due to the solubility of Alq₃ in chloroform, the chloroform concentration is able to increase to the point of dissolving the Alq₃ globules and microcrystallites. Since solubility decreases with increasing size, the larger crystalline needles do not dissolve, but rather grow at the expense of the submicron residual Alq₃ structures (i.e., via Ostwald ripening). When the Regime I residual Alq₃ dissolves, the solvated Alq₃ begins to wet the substrate as evidenced by the shapes of the Regime II strips and droplets (Figs. 3(c), (d) and 4(e)). This wetting behavior is consistent with the observed spreading of a drop of neat chloroform on an OTS-treated substrate.

Although the morphological transition from Regime I globules/microcrystallites to Regime II fluid-like strips/droplets can be effected by increased annealing time, as illustrated in Fig. 4, the coexistence of both regimes on a single substrate (Fig. 3) suggests that other factors influence the local chloroform concentration. For example, the exclusion of chloroform when Alq₃ molecules crystallize at the needle/solution interface would result in an increase in chloroform concentration near the needle. This would explain the observed collocation of Regime II regions containing liquescent Alq₃ (i.e., high chloroform concentration) and the Alq₃ needles. In fact, needle growth not only contributes to but also benefits from the increased local chloroform concentration, since needle growth relies on transport of Alq₃ to the needle/solution interface and in general transport is facilitated by an increase in fluidity. Moreover, the submicron grating grooves provide a means for capillary flow of liquescent Alq₃, greatly enhancing the transport of Alq₃ along the grooves [41]. The resulting anisotropic mass transport is evidenced by elongation of the Regime II “flow regions” in the grating direction (Fig. 1(b)) and is responsible for growth of the needles parallel to the grating direction.

5. Conclusions

In summary, we have formed millimeter-scale crystalline Alq₃ needles via room temperature solvent-vapor exposure of initially amorphous thin

films on patterned substrates. The remarkable size of the needles results from enhanced mass transport due to (1) the solubility of Alq₃ in chloroform and (2) capillary flow along the substrate grooves. The crystallization method has been demonstrated for Alq₃ thin films annealed in chloroform vapor, but is expected to be generally applicable to other material/solvent/substrate systems. An understanding of the crystal seeding process, which would enable placement of the oriented needles at specified locations on a substrate, will be valuable in optimizing the method for potential device fabrication. Organic crystalline needles generated via this technique may have enhanced charge carrier mobilities necessary for organic electronic applications such as low-voltage field-effect transistors and high-efficiency solar cells, or non-linear optical properties required for organic optoelectronic devices such as modulators, optical filters, and polarization rotators.

Acknowledgements

We thank C.A. Breen, J. Chen, S.A. Claussen, I. Kymissis, C.F. Madigan, M.E. Walsh, and J.J. Zartman for technical assistance, and T.M. Swager for technical discussions. We received support for this work from the MARCO Focused Research Center on Materials, Structures, and Devices which is funded at the Massachusetts Institute of Technology, in part by MARCO under contract 2001-MT-887 and DARPA under grant MDA972-01-1-0035. This work made use of the Shared Experimental Facilities supported in part by the MRSEC Program of the National Science Foundation under award number DMR 02-13282.

References

- [1] C.D. Dimitrakopoulos, P.R.L. Malenfant, *Adv. Mater.* 14 (2002) 99.
- [2] H.E. Katz, Z. Bao, *J. Phys. Chem. B* 104 (2000) 671.
- [3] Y.Y. Lin, D.J. Gundlach, S.F. Nelson, T.N. Jackson, *IEEE Trans. Electron Dev.* 44 (1997) 1325.
- [4] P. Peumans, V. Bulović, S.R. Forrest, *Appl. Phys. Lett.* 76 (2000) 2650.
- [5] S.R. Marder, J.W. Perry, C.P. Yakymyshyn, *Chem. Mater.* 6 (1994) 1137.
- [6] F. Iwatsu, T. Kobayashi, N. Uyeda, *J. Phys. Chem.* 84 (1980) 3223.
- [7] F. Iwatsu, *J. Cryst. Growth* 71 (1985) 629.
- [8] A.M. Hor, R.O. Loutfy, *Thin Solid Films* 106 (1983) 291.
- [9] B.A. Gregg, *J. Phys. Chem.* 100 (1996) 852.
- [10] J.C. Conboy, E.J.C. Olson, D.M. Adams, J. Kerimo, A. Zaban, B.A. Gregg, P.F. Barbara, *J. Phys. Chem. B* 102 (1998) 4516.
- [11] M. Brinkmann, J.C. Wittmann, C. Chaumont, J.J. Andre, *Thin Solid Films* 292 (1997) 192.
- [12] F. Toffolo, M. Brinkmann, O. Greco, F. Biscarini, C. Taliani, H.L. Gomes, I. Aiello, M. Ghedini, *Synth. Met.* 101 (1999) 140.
- [13] F.R. Lipsett, *Can. J. Phys.* 35 (1957) 284.
- [14] F. Gutmann, L.E. Lyons, *Organic Semiconductors*, John Wiley & Sons, Inc., New York, 1967.
- [15] D. Fichou, *J. Mater. Chem.* 10 (2000) 571.
- [16] C. Kloc, P.G. Simpkins, T. Siegrist, R.A. Laudise, *J. Cryst. Growth* 182 (1997) 416.
- [17] R.A. Laudise, C. Kloc, P.G. Simpkins, T. Siegrist, *J. Cryst. Growth* 187 (1998) 449.
- [18] G. Horowitz, B. Bachet, A. Yassar, P. Lang, F. Demanze, J.L. Fave, F. Garnier, *Chem. Mater.* 7 (1995) 1337.
- [19] M. Pope, H.P. Kallmann, P. Magnante, *J. Chem. Phys.* 38 (1963) 2042.
- [20] G. Horowitz, F. Garnier, A. Yassar, R. Hajlaoui, F. Kouki, *Adv. Mater.* 8 (1996) 52.
- [21] V. Podzorov, V.M. Pudalov, M.E. Gershenson, *Appl. Phys. Lett.* 82 (2003) 1739.
- [22] F. Pan, K. McCallion, M. Chiappetta, *Appl. Phys. Lett.* 74 (1999) 492.
- [23] J.F. Moulin, M. Brinkmann, A. Thierry, J.C. Wittmann, *Adv. Mater.* 14 (2002) 436.
- [24] E.L. Granstrom, C.D. Frisbie, *J. Phys. Chem. B* 103 (1999) 8842.
- [25] W.A. Schoonveld, J. Vrijmoeth, T.M. Klapwijk, *Appl. Phys. Lett.* 73 (1998) 3884.
- [26] G.Z. Wang, Y. Luo, P.H. Beton, *Appl. Phys. Lett.* 83 (2003) 3108.
- [27] C.D. Dimitrakopoulos, A.R. Brown, A. Pomp, *J. Appl. Phys.* 80 (1996) 2501.
- [28] Z. Bao, A.J. Lovinger, A. Dodabalapur, *Appl. Phys. Lett.* 69 (1996) 3066.
- [29] Y.L. Lee, W.C. Tsai, C.H. Chang, Y.M. Yang, *Appl. Surf. Sci.* 172 (2001) 191.
- [30] D.J. Gundlach, T.N. Jackson, D.G. Schlom, S.F. Nelson, *Appl. Phys. Lett.* 74 (1999) 3302.
- [31] C.W. Tang, S.A. Vanslyke, *Appl. Phys. Lett.* 51 (1987) 913.
- [32] E.M. Han, L.M. Do, N. Yamamoto, M. Fujihira, *Thin Solid Films* 273 (1996) 202.
- [33] K. Naito, A. Miura, *J. Phys. Chem.* 97 (1993) 6240.
- [34] H.I. Smith, M.W. Geis, C.V. Thompson, H.A. Atwater, *J. Cryst. Growth* 63 (1983) 527.
- [35] T. Kobayashi, K. Takagi, *Appl. Phys. Lett.* 45 (1984) 44.

- [36] D.C. Flanders, D.C. Shaver, H.I. Smith, *Appl. Phys. Lett.* 32 (1978) 597.
- [37] J.Y. Cheng, C.A. Ross, E.L. Thomas, H.I. Smith, G.J. Vancso, *Appl. Phys. Lett.* 81 (2002) 3657.
- [38] M. Brinkmann, G. Gadret, M. Muccini, C. Taliani, N. Masciocchi, A. Sironi, *J. Am. Chem. Soc.* 122 (2000) 5147.
- [39] J. Bicerano, *Prediction of Polymer Properties*, Marcel Dekker, Inc., New York, 1996.
- [40] C.F. Madigan, V. Bulović, unpublished work.
- [41] R. Seemann, M. Brinkmann, E.J. Kramer, F.F. Lange, R. Lipowsky, *Proc. Natl. Acad. Sci. USA* 102 (2005) 1848.